Proceedings of the 4th International Conference on Mechatronics and Smart Systems
DOI: 10.54254/2755-2721/2026.33010

Umbrella-Based Deployable Tensegrity Wheel

Chenlei Guo[1†], Jiacheng Ye[2*†]

[1]*Reading Academy, Nanjing University of Information Science and Technology, Nanjing, China*
[2]*College of Engineering, University of Connecticut, Storrs, USA*
**Corresponding Author. Email: Jiacheng.ye@uconn.edu*
[†]*These authors contributed equally to this work and should be considered co-first authors.*

Abstract. This paper primarily investigates the feasibility of folding wheels in tensioned structures, emphasizing the rationale for employing umbrella-shaped structures and presenting relevant mechanical analyses. The proposed deployable tensegrity wheel uses a single-degree-of-freedom hub slider to coordinate perimeter cables, enabling reversible folding and diameter adjustment during operation while maintaining pre-tension. A compact kinematic model relates slider travel to wheel diameter and rope length, and a node-level force balance explains how folding increases structural compliance and contact length. These analyses lead to a terrain-dependent usage rule: the largest diameter is preferred for clearance and obstacles, an intermediate diameter for loose ground, and the smallest diameter for narrow passages. A physical prototype was manually operated to confirm smooth, continuous transitions between the fully deployed, half-folded, and fully folded configurations—all without requiring disassembly or reassembly. These results demonstrate that deployable tensegrity wheels are not only feasible but also represent a compact, mass-efficient, and terrain-adaptive non-pneumatic mobility solution, particularly suited for planetary missions where stowage space is limited and traction demands are unpredictable.

Keywords: tensegrity, deployable, foldability, octagonal, umbrella, wheel

1. Introduction

1.1. Source of tensegrity

Of course, the story of "tensegrity" doesn't start in a lab or on a whiteboard — it really began with art. Back in the 1950s, the architect and thinker Buckminster Fuller noticed something special in the sculptures of Kenneth Snelson: rigid struts that seemed to float, suspended within delicate networks of stainless steel cables. Fuller coined the term — blending tension and integrity — to capture the essence of structures that balance compression and tension in a state of graceful equilibrium. It's almost poetic how these structures work — there's no glue, no welding, just pure balance. What looks fragile is in fact deceptively strong and incredibly efficient. Tensegrity doesn't fight forces; it guides them. That's why such systems aren't just theoretical marvels — they've become practical solutions where both weight and durability matter. Today, you'll find tensegrity at work in everything from collapsible robotic systems and spacecraft components to exploration rovers built for distant planets — machines that must be both lightweight and tough enough for the unknown. There's something almost visionary about the idea — simple in principle, yet radical in its potential [1].

© 2026 The Authors. This is an open access article distributed under the terms of the Creative Commons Attribution License 4.0 (https://creativecommons.org/licenses/by/4.0/).

DOI: 10.54254/2755-2721/2026.33010

1.2. Design and analysis of a deployable tensegrity wheel for planetary rovers

When it comes to extraterrestrial exploration—such as lunar or Martian missions—rovers face extreme and unpredictable environmental challenges. They must navigate rugged, rocky terrain, withstand drastic temperature swings, and operate reliably in low-gravity and near-vacuum conditions. Conventional pneumatic tires, which depend on internal air pressure for support and performance, are ill-suited for these scenarios. They are vulnerable to punctures, material degradation, and pressure loss in vacuum environments, imposing serious limitations [2, 3]. As a result, significant research effort has shifted toward developing non-pneumatic, compliant wheel systems that can undergo repeated elastic deformation while maintaining structural integrity and traction on challenging planetary surfaces [4].

Tensegrity-based wheels have surfaced as a promising alternative in this domain. Owing to their reconfigurable and compliant nature, tensegrity wheels can conform to irregular surfaces while providing shock absorption and shape recovery. NASA has previously explored analogous technologies, such as the Spring Tire—developed in partnership with Goodyear—and the superelastic tire constructed from shape memory alloys, both conceived to overcome the shortcomings of conventional wheels in space exploration [5, 6]. Integrating tensegrity principles into rover wheel design facilitates structures that are not only lightweight and collapsible for compact transport but also highly resilient and adaptive to varying terrain during operation. Recent advances further reveal that deployable tensegrity wheels possess active shape-morphing capabilities [7], enabling real-time adjustment of wheel diameter through controlled cable length variation. This functionality allows the wheel to modify its ground contact geometry, enhancing adaptability across diverse terrains. Experimental evidence indicates that such wheels exhibit robust performance over varied surfaces, including grass, foliage, sand, rock, snow, and ice (Figure 1). This multi-terrain traversability underscores the potential of tensegrity-based wheels for missions requiring versatile ground interaction. Although the coordination of deformation mechanisms and structural integrity maintenance entail considerable design complexity, the advantages of light weight, deployability, and load-adaptive robustness position deployable tensegrity wheels as a strong candidate for next-generation rover mobility systems.



Figure 1. High trafficability of a deployable tensegrity wheel [7]

1.3. Overview introduction

This paper conducts a foldability analysis of a two-dimensional deployable tensegrity wheel, emphasizing its capacity to transition between varying diameters during folding. The research examines how such diameter-switching mechanisms can enhance the adaptability of rover wheels to the diverse terrains encountered in planetary exploration missions.

2. Umbrella based tensegrity design

Tensegrity structures can be constructed in a variety of ways to serve diverse purposes. In order to enhance their adaptability to various terrains, we have conducted research on the formation methods

DOI: 10.54254/2755-2721/2026.33010

of tensegrity structures. These structures can be created by exploring the topology of tensegrity families or by investigating the optimal design of active tensegrity structures through topology optimization [8]. Other examples include the soft umbrella-like tensegrity robot [9], the deployable aerodynamic decelerator [10], the heavy-load variable stiffness lunar wheel [11], and the shape-changing wheeling and jumping robot [7]. After a thorough evaluation of these options, we ultimately decided to construct a rimless wheel, as depicted in Fig. 2, which can simulate the simplest walking model of the forelimbs or hindlimbs of quadrupeds [12].

2.1. Structural configuration: components and geometric features of the 2D tensegrity wheel

The design of the proposed 2D deployable tensegrity wheel is inspired by the principles of tensional integrity, in which isolated compressive members are suspended within a continuous network of tensile elements. In this configuration, the blue components represent rigid struts (rods) that resist compression, while the red components represent tensile cables or strings that maintain the structural integrity of the system through pre-tensioning. (Figure 2)

The overall geometry forms an eight-pointed star, consisting of an outer ring of nodes connected by tension elements, and an internal cross-laced system of rods that span between non-adjacent nodes. This layout achieves geometric balance and allows for radial symmetry, which is crucial for even force distribution and structural stability during deformation and deployment. (Figure 2)

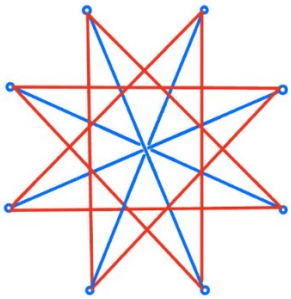


Figure 2. Octagonal tensile structure

2.2. Force analysis

Since the forces acting on each vertex of the octagonal tensioning structure are similar, the analysis herein focuses on point A, as illustrated in Figure 3. To understand the mechanical behavior of the deployable tensegrity wheel, a simplified force analysis is conducted at this representative outer node. Figure 3 provides an enlarged view of node A, where multiple structural elements converge: one compressive strut (indicated in blue) and two tensile cables (shown in red). This arrangement is characteristic of the geometry throughout the outer ring of the wheel.

At node A, the compressive strut exerts an upward reaction force $\boldsymbol{F}$, while the two symmetric tensile cables apply forces of magnitude $\boldsymbol{T}$ along their respective axes. Under the assumption of static equilibrium, the vertical components of the tensile forces must balance the upward compressive force. This yields the following equilibrium condition:

$$F = 2T \times cos\,\theta \tag{1}$$

where θ denotes the angle between each tensile member and the vertical axis. The system maintains tensional integrity, meaning the cables remain exclusively in tension, and the compressive struts are subject solely to axial compression, without sustaining bending moments.

DOI: 10.54254/2755-2721/2026.33010

This triangular force distribution ensures stability and load transfer efficiency within the wheel structure. Due to the symmetry of the layout, similar force patterns are repeated around the wheel, which allow it to uniformly absorb external loads from ground contact or deformation. This structural behavior underlies the wheel's ability to passively conform to terrain irregularities while maintaining its shape through internal force balance.

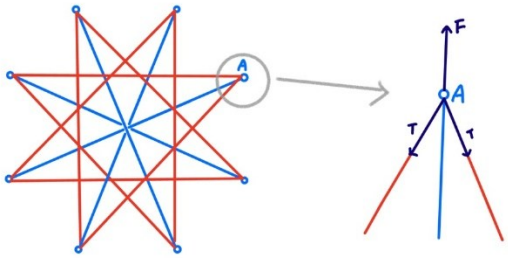


Figure 3. Octagonal tensile structure force analysis

2.3. Foldability and deployability

The proposed two-dimensional tensegrity wheel consists of rigid compressive struts (depicted in blue) and pre-tensioned cables (shown in red), arranged in a symmetric eight-point star configuration. The struts bear compressive loads to ensure structural stability, while the tensile cables preserve the geometric configuration and enable precise deformation control through adjustable tension. This configuration achieves a balance between lightweight design and structural strength, rendering it highly suitable for planetary mobility applications.

An essential feature of this design is the deployability, which enables the wheel to adapt its diameter in response to varying terrain conditions. Drawing inspiration from the mechanical principle of an umbrella, the structure achieves radial folding through a hinged strut system and a central sliding mechanism. In Figure 4, this configuration allows the wheel to collapse compactly for storage or deploy into a functional form. Similarly, in the tensegrity wheel, actuation—such as tensioning internal cables or adjusting the central hub—drives the structure to fold inward, reducing its overall size, or expand outward into a stable, operational configuration suitable for rolling.

This folding mechanism not only facilitates space-efficient storage but also enables dynamic wheel-size adjustment during operation. This adaptability is particularly beneficial for off-Earth rovers that must navigate a variety of terrain conditions, from soft soil and loose sand to tight crevices or rocky slopes. By dynamically changing its diameter, the wheel can optimize traction and clearance depending on environmental needs.

The simplified 2D construction enhances fabrication feasibility and control, serving as a foundational prototype for more complex three-dimensional deployable tensegrity structures. Overall, the wheel's structure integrates mechanical efficiency, symmetry, and transformability, making it a viable design for future deployable planetary mobility platforms.

DOI: 10.54254/2755-2721/2026.33010

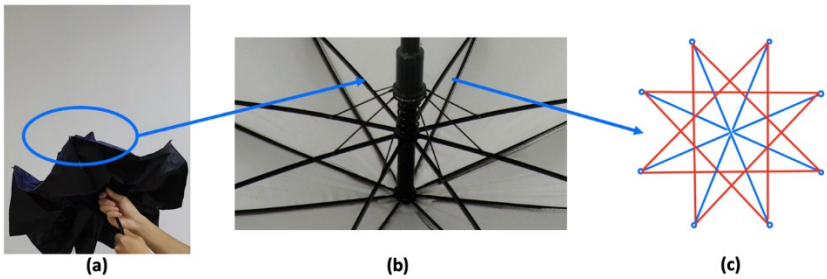


Figure 4. (a)Convenient storage of umbrella, (b)The structure of umbrella frame, (c)A similar tensegrity structure

3. Numerical and geometric analysis

3.1. Introduction

The deployable tensegrity wheel comprises three key components: rigid bars, tension ropes, and a rotational assembly. The rigid bars primarily bear compressive forces, while the ropes remain under tension. To regulate the wheel's diameter while maintaining tension control, the central rotational assembly is actuated to adjust the rope length. Additionally, a braking mechanism is integrated at the sliding interface between the slider and the central axis to lock the desired configuration. The model is just like the way a retractable umbrella deploys and retracts.

In the physical prototype, wheel diameter control is achieved through rotation of the central assembly. We define the rotation angle as α and the resulting wheel diameter as D. Critically, maintaining structural tension during diameter adjustment requires coordinated shortening of the cable length (denoted as Y). This study first establishes the mathematical relationships between D and α, as well as Y and α, then focuses on analyzing the mechanical behavior during dynamic diameter transitions.

3.2. Geometric analysis

Figure 5(a) illustrates the geometric configuration of our system, where the rotation assembly is positioned at the intersection point between the central axis and the vertical height dimension. If point A is taken as the origin, then the position of the rotation assembly slider on the rotating shaft, denoted as x_c, satisfies the equation

$$x_c^2 + D^2 = L_1^2 \quad or \quad x_c = \sqrt{L_1^2 - D^2} \tag{2}$$

The structural components form triangle ABC, with defined lengths: AB = L_1 (constant), BC = L_2 (constant), and AC = x (variable). The angle between segments L_1 and the horizontal axis is denoted as θ. Figure 5(b) illustrates the relation between the diameter and the whole rope length Y while keeping tension. With these two figures we can find three functions $D(\alpha)$, $Y(\alpha)$ and $x(\alpha)$.

Assume axis radius is r, the maximum diameter of wheel is D_0 directly we know that

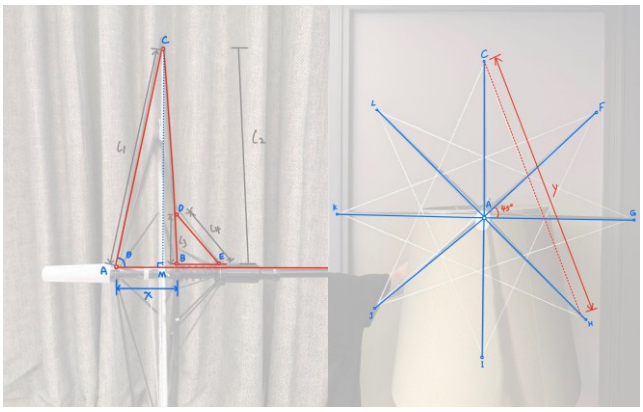
$$D_0 - D = \alpha r \tag{3}$$

where $D \leq D_0$ and $\alpha > 0$. From figure 5(b) we can know that the rope has 9 parts the relation between Y and D can be found that

$$Y = k_1 D \tag{4}$$

DOI: 10.54254/2755-2721/2026.33010

where $k_1 = (8\sqrt{2+\sqrt{2}}+1)$.



(a) (b)

Figure 5. (a) Shows one of eight part the model of wheel structure, (b) shows top view of the whole structure

To know the function $x(\alpha)$ simplify the following equations

$$\begin{cases} D_0 - D = \alpha r \\ D = L_1 sin\theta \\ cos\theta = \dfrac{L_1^2 + x^2 - L_2^2}{2xL_1} \end{cases} \tag{5}$$

we get

$$x^2(\alpha) = 2\left(\left(D_0 - \alpha r\right)^2 - L_1 L_2\right) \pm \sqrt{4\left(L_1 L_2 - (D_0 - \alpha r)^2\right)^2 + \left(L_1^2 + L_2^2\right)^2} \tag{6}$$

In the physics model, L_1, L_2 and D_0 are approximately equal and significantly larger than r, the appropriate choice for inner sign is the positive one. Thus, we get

$$x(\alpha) = \sqrt{2\left(\left(D_0 - \alpha r\right)^2 - L_1 L_2\right) + \sqrt{4\left(L_1 L_2 - (D_0 - \alpha r)^2\right)^2 + \left(L_1^2 + L_2^2\right)^2}} \tag{7}$$

$$D(\alpha) = D_0 - \alpha r \tag{8}$$

$$Y(\alpha) = k_1\left(D_0 - \alpha r\right) \tag{9}$$

3.3. Force analysis

The following analysis is on the situation the wheel keeping off the ground. The tensegrity wheel is a central symmetry structure, while changing the diameter the force on bars will change with the change of geometric relationship

DOI: 10.54254/2755-2721/2026.33010

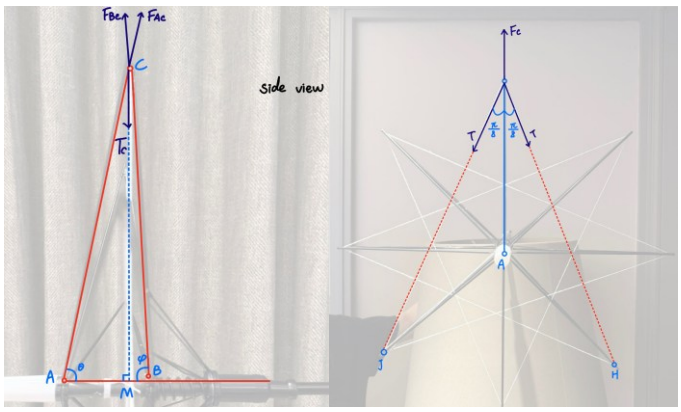
In figure 6, to unify the standards we first denote the angle $\angle B_1AC$ as θ and $\angle B_1CA$ as φ, than the force on two bars called F_{AB_1} and F_{CB_1} the force balance equation. The prepress on the rope is denoted as T. Now we can find the force balance equations that

$$\begin{cases} F_{AB_1}cos\theta = F_{CB_1}cos\varphi \\ F_{AB_1}cos\theta + F_{CB_1}cos\varphi = 2Tcos\dfrac{\pi}{8} \\ cos\theta = \dfrac{L_1^2 + x^2 - L_2^2}{2xL_1} \\ cos\varphi = \dfrac{L_2^2 + x^2 - L_1^2}{2xL_2} \end{cases} \tag{10}$$

We get the two functions $F_{AB_1}(x,T)$ and $F_{CB_1}(x,T)$

$$F_{AB_1}(x,T) = T\sqrt{2+\sqrt{2}}\frac{L_2\left(L_1^2 - L_2^2 + x^2\right)}{x\sqrt{\left(\left(L_1+L_2\right)^2 - x^2\right)\left(x^2 - \left(L_1 - L_2\right)^2\right)}} \tag{11}$$

$$F_{CB_1}(x,T) = T\sqrt{2+\sqrt{2}}\frac{L_1\left(-L_1^2 + L_2^2 + x^2\right)}{x\sqrt{\left(\left(L_1+L_2\right)^2 - x^2\right)\left(x^2 - \left(L_1 - L_2\right)^2\right)}} \tag{12}$$



(a) (b)

Figure 6. (a) The force analysis form side view to one of eight part, (b) the force analysis form top view

Figure 7 illustrates the connection between a vertex and the rotational assembly. The setup is similar to Figure 6, with the key difference being an additional segment of rope passing through point B. We can find another force balance equations that

DOI: 10.54254/2755-2721/2026.33010

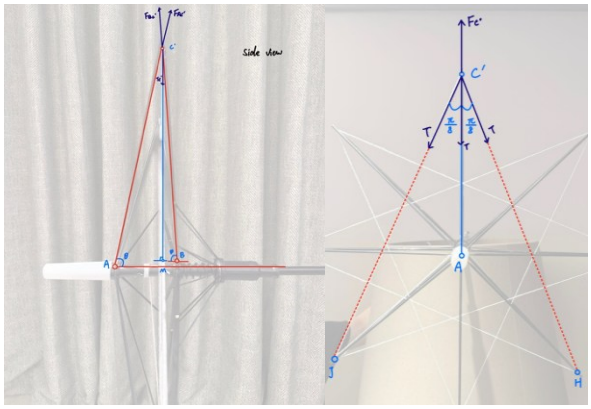
$$\begin{cases} F_{AB_2}cos\theta = F_{CB_2}cos\varphi \\ F_{AB_2}cos\theta + F_{CB_2}cos\varphi = 2Tcos\dfrac{\pi}{8} + T \end{cases} \tag{13}$$

We get the two similar functions $F_{AB_2}(x,T)$ and $F_{CB_2}(x,T)$

$$F_{AB_2}(x,T) = T(1+\sqrt{2+\sqrt{2}})\frac{L_2\left(L_1^2 - L_2^2 + x^2\right)}{x\sqrt{\left(\left(L_1+L_2\right)^2 - x^2\right)\left(x^2 - \left(L_1 - L_2\right)^2\right)}} \tag{14}$$

$$F_{CB_2}(x,T) = T(1+\sqrt{2+\sqrt{2}})\frac{L_1\left(-L_1^2 + L_2^2 + x^2\right)}{x\sqrt{\left(\left(L_1+L_2\right)^2 - x^2\right)\left(x^2 - \left(L_1 - L_2\right)^2\right)}} \tag{15}$$

With equation (6) we can find $F_{AB_1}(\alpha,T)$, $F_{CB_1}(\alpha,T)$, $F_{AB_2}(\alpha,T)$ and $F_{CB_2}(\alpha,T)$. Notice that when $x = L_2^2 - L_1^2$, F_{CB_1} will be 0 which means that BC is vertical to AC, but the situation cannot happen otherwise the system will lock itself, so as F_{CB_2}.



(a) (b)

Figure 7. (a)(b) Show the connect part with on more part of rope

Figure 8 depicts the scenario where the rotational assembly is displaced from its equilibrium position x_c. In this case, the system becomes unstable and experiences a horizontal force $F_c = Tsin\beta$,
where β represents the angular deviation of the rope from the vertical axis.

DOI: 10.54254/2755-2721/2026.33010

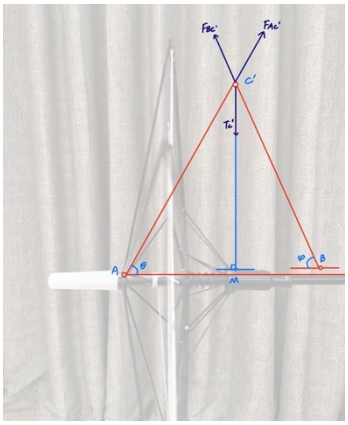


Figure 8. The situation of the central rotation assembly is not at stable position

4. Models

4.1. Prototype and actuation

The prototype is a two-dimensional tensegrity wheel composed of rigid struts and perimeter cables arranged in an eight-point star. Diameter control is realized by an umbrella-like slider at the hub that synchronously shortens/lengthens the perimeter cables while preserving a closed tension network. Consistent with the geometric model in Sec. 3, the commanded rotation α of the central assembly maps to wheel diameter and total rope length, ensuring that pre-tension is maintained throughout the motion.

4.2. Operational morphologies and diameter switching

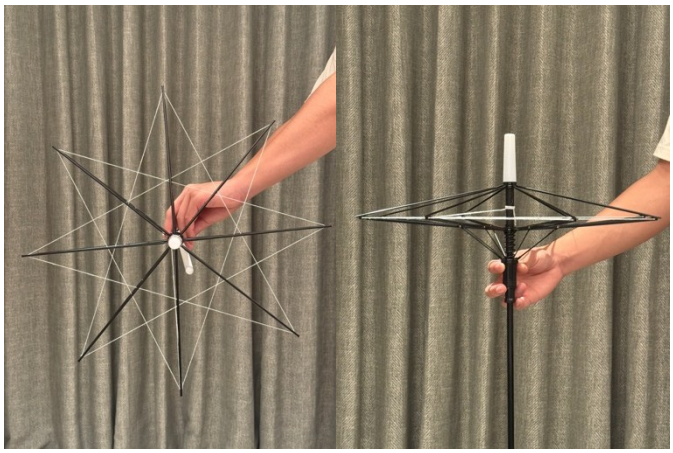
Figures 9–11 document three rollable morphologies produced by a single continuous motion of the slider.

- Fully deployed (Fig. 9, $D \approx D$ max). Largest diameter and ground clearance; higher radial stiffness; suited to obstacles and coarse terrain.
- Half-folded (Fig. 10, $D = D$ mid). Intermediate diameter: increased compliance and longer contact length; improved traction on yielding substrates with moderate clearance.
- Fully folded (Fig. 11, $D \approx D$ min). Minimum diameter, compact cross-section; lowest traversal height but lowest rolling torque on firm ground; advantageous for narrow passages.

Across these states the structure remains self-stressed and kinematically unobstructed (no cable slack or hinge locking), enabling reversible, on-the-fly diameter switching without reassembly.

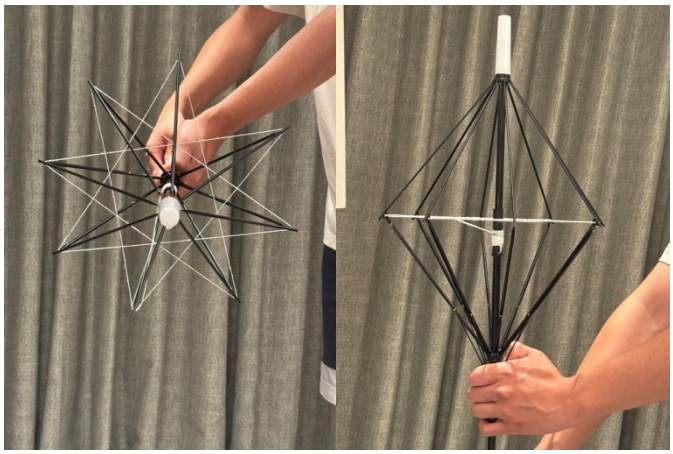
This enables the wheel to adapt to different terrain conditions—such as narrow crevices, soft sand, or rough rocks—by either compressing for passage or expanding to increase contact area and traction.

DOI: 10.54254/2755-2721/2026.33010



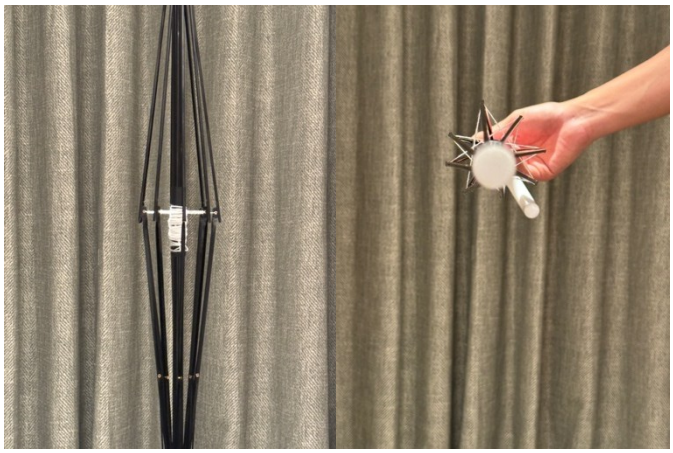
(a) (b)

Figure 9. Prototype in the fully deployed state (D max)



(a) (b)

Figure 10. Prototype in the half-folded state (D mid)



(a) (b)

Figure 11. Prototype in the fully folded state (D min)

DOI: 10.54254/2755-2721/2026.33010

4.3. Qualitative behavior and design trade-offs

The observed behavior aligns with the force paths in Sec. 2.2: outer-node equilibrium

F = 2T × cos (θ) implies that, as the wheel folds and θ increases, vertical support per cable decreases

and global compliance rises. Consequently:

- Increasing D raises obstacle-clearing capacity and radial stiffness, but also the required drive torque.
- Decreasing D reduces torque demand and improves maneuverability in confined spaces, at the cost of reduced clearance.
- Contact length scales monotonically with compliance in the half-folded regime, which benefits traction on sand or snow.

These trade-offs motivate diameter scheduling as a terrain-aware control policy: use D max for rocks/steps, D mid for loose media, and D min for gaps and tight corridors.

5. Conclusion

This paper introduced an umbrella-inspired deployable tensegrity wheel and a diameter-switching mechanism that preserves pre-tension during folding. We formulated geometric relationships between actuation angle, wheel diameter, and rope length; established outer-node force balance to explain stiffness/compliance trends; and demonstrated a physical prototype operating in three rollable morphologies (fully deployed, half-folded, fully folded). Collectively, these results support the use of tensegrity wheels as lightweight, terrain-adaptive, non-pneumatic mobility solutions for planetary rovers.

Even so, several critical performance dimensions remain unexamined due to the prototype's manual actuation and laboratory-bound evaluation. Our immediate trajectory will address these gaps through systematic experimentation and design refinement. Due to the limited scope of the experiment, we have not yet tested:

The relationship between preload and overall stiffness. While the geometric model (Fig. 3) assumes a constant pre-tension T, the empirical mapping between cable preload and the wheel's radial stiffness—particularly under dynamic loading—remains uncharacterized. Future work will implement a load cell–instrumented tensioning system to quantify how variations in T affect both static compliance and vibration-damping behavior during rolling, thereby enabling stiffness scheduling as an active control input for terrain-specific optimization.

Wheel traction force, energy consumption, and traversal capability. The present analysis focuses on off-ground kinematics; however, real-world mobility necessitates understanding how diameter morphing influences drawbar pull on loose regolith, rolling resistance on rigid substrates, and power efficiency across morphological transitions. We will deploy the wheel on a variable-inclination terrain mockup instrumented with a towing dynamometer and wattmeter to capture traction-slip curves and energy-per-distance metrics for each operational morphology depicted in Figs. 9–11.

Electric drive. The central rotation assembly is manually driven now; however, it can be replaced by a slidable motor which can take the rope in while sliding on the axis. A compact, cable-driven servo motor integrated with a lead-screw slider will be developed to enable autonomous, closed-loop diameter adjustment. This electromechanical system will incorporate encoder feedback to correlate commanded rotation angle α with actual diameter D, ensuring precise morphological control under onboard computational guidance.

Temperature effects. Planetary environments impose extreme thermal cycles that may alter cable elasticity, joint friction, and material creep. Future prototypes will incorporate stainless-steel cables

DOI: 10.54254/2755-2721/2026.33010

and titanium alloy struts, then undergo thermal-vacuum chamber testing to evaluate tension retention and deployment repeatability across –150 °C to +120 °C, representative of lunar polar and Martian equatorial conditions.

Redundancy design. The wheel may not be suitable for all situations because redundancy is not considered in the wheel. To enhance fault tolerance for long-duration missions, we will explore a dual-cable-per-edge topology with asymmetric pre-tensioning, allowing the structure to maintain functionality even after a single cable fracture. Monte Carlo failure-mode simulations will guide the placement of redundant load paths without incurring prohibitive mass penalties. These points will be addressed in future experiments to gather additional data, culminating in a fully integrated, terrain-aware mobility platform capable of autonomous diameter adaptation under realistic extraterrestrial analog conditions.

References

[1] Snelson, Kenneth. “The Art of Tensegrity.” International Journal of Space Structures, vol. 27, no.2-3, June 2012, pp. 71–80.
[2] Heverly, M., et al. (2013). Mars Science Laboratory wheel design and performance. In 10th International Symposium on Artificial Intelligence, Robotics and Automation in Space (i-SAIRAS).
[3] Dubowsky, S., et al. (2008). Mobility and manipulation for planetary exploration robots. In Smart Structures and Materials 2008: Electroactive Polymer Actuators and Devices (EAPAD).
[4] Jansen, J., et al. (2010). Non-pneumatic tire concepts for lunar and Martian terrain. SAE Technical Paper 2010-01-0155.
[5] Clark, A., & Dubowsky, S. (2010). Tensegrity wheels for planetary exploration. ASME International Design Engineering Technical Conferences.
[6] Martinez, J. M., et al. (2017). The NASA super elastic Tire: A Non-Pneumatic Tire for Future Mars Rovers. NASA Technical Report NASA/TM–2017-219573.
[7] Spiegel, Sydney, et al. “A Shape-Changing Wheeling and Jumping Robot Using Tensegrity Wheels and Bistable Mechanism.” IEEE-ASME Transactions on Mechatronics, vol. 28, no. 4, 1 Aug. 2023, pp. 2073–2082, https://doi.org/10.1109/tmech.2023.3276933.
[8] Wang, Y., Han, Z., Xu, X., & Luo, Y. (2024). Topology optimization of active tensegrity structures. Computers & Structures, 305, 107513.
[9] Liu, Y., Zhang, Y., Dai, X., Wu, R., Zhang, Z., Li, Y., & Zhao, J. (2025). SUTBot: A Soft Umbrella-like Tensegrity Robot with Elastic Struts for In-pipe Locomotion. IEEE Robotics and Automation Letters.
[10] Xu, W. X., Zhang, J., Guo, H. W., Liu, R. Q., & Kou, Z. M. (2024). Design of a deployable aerodynamic decelerator based on a tensegrity structure. Acta Astronautica, 215, 315-324.
[11] Zhao, S., Zhang, X., Zhang, Z., Bao, L., & Guo, Q. (2025). Heavy-load variable stiffness lunar wheel based on adjustable tensegrity unit. Journal of Terramechanics, 120, 101074.
[12] Xiang, Y., Zheng, Y., & Asano, F. (2024, May). Modeling and analysis of combined rimless wheel with tensegrity spine. In 2024 IEEE International Conference on Robotics and Automation (ICRA) (pp. 8088-8093). IEEE.